Desalination and Water Treatment
www.deswater.com
doi: 10.5004/dwt.2023.29638

296 (2023) 71–82
June

Poly(4-styrene sulfonic acid) resin for heavy metal ions adsorption: characterization, adsorption properties, thermodynamic and reusability studies

Youning Chen*, Min Wang, Shuang Jia, Yuhong Li, Xiaohua Meng, Xiaoling Yang

College of Chemistry and Chemical Engineering, Xianyang Normal University, Xianyang 712000, China, emails: cyn5363@163.com (Y.N. Chen), 1831365645@qq.com (M. Wang), 2477752442@qq.com (S. Jia), 309943006@qq.com (Y.H. Li), 914297288@qq.com (X.H. Meng), 504248504@qq.com (X.L. Yang)

Received 5 January 2023; Accepted 11 May 2023

ABSTRACT

A novel poly(4-styrene sulfonic acid)-graft resin (PSS-g-PS) with high adsorption capacity was prepared by grafting poly(4-styrene sulfonic acid) (PSS) onto chloromethylated styrene resin via surface-initiated atom transfer radical polymerization. The surface composition of the poly(4-styrene sulfonic acid)-grafted resin were characterized by Fourier-transform infrared spectrometry, scanning electron microscopy, energy-dispersive X-ray spectroscopy and X-ray photoelectron spectroscopy. It was found that the grafting amount of 4-styrenesulfonic acid increased linearly with the polymerization time. Effect of parameters such as pH, initial concentration and temperature on the removal of heavy metal ions was studied. The maximum adsorption capacities of the resin were up to 275 $mg \cdot g^{-1}$ for Pb(II), 169 $mg \cdot g^{-1}$ for Cu(II), 115 $mg \cdot g^{-1}$ for Cd(II), 90.8 $mg \cdot g^{-1}$ for Cr(III) and 75 $mg \cdot g^{-1}$ for Ni(II) at pH 5.0. The adsorption isotherms of the five metal ions were best described by the Langmuir model, and their adsorption kinetics followed the pseudo-second-order kinetic equation. Thermodynamic studies showed that the adsorption was spontaneous. Furthermore, the resins still maintained good adsorption capacity after 10 cycles of adsorption–regeneration. All the results suggested that the resin could be potentially applied to the efficient removal of heavy metal ions from wastewater.

Keywords: Poly(4-styrene sulfonic acid) grafted-chloromethylated polystyrene resin; Heavy metal ion; Adsorption

1. Introduction

The massive discharge of metal polluted industrial wastewater caused serious pollution of water, soil and food by heavy metal ions (such as Cd, Cr, Cu, Ni, As, Pb and Zn) [1,2]. Due to its high solubility in water, heavy metal ions are absorbed by organisms and enter the ecosystem. After being amplified by the food chain, they are gradually enriched in higher-level organisms, causing adverse reactions at various levels in the ecosystem, and endangers the health and survival of various life forms, including the human body [3–5]. Therefore, the problem of industrial wastewater treatment has increasingly attracted the attention of researchers at home and abroad in recent years [6,7]. There are many methods to remove heavy metal ions in wastewater, including chemical precipitation/coagulation method [8], membrane technology method [9], electrolytic reduction method [10], ion-exchange method [11] and adsorption method [12]. Among all these treatment methods, the adsorption method has become an important physicochemical method in heavy metal ion industrial wastewater treatment because of its advantages of low-cost, good effect, and strong operability [13–15]. In the process of heavy metal ion industrial wastewater treatment, the use of high-performance adsorbents is the key to improving the water treatment effect [16,17].

* Corresponding author.

Generally, the surface of all solid materials has an adsorption effect. In fact, only porous materials with a large specific surface area and corresponding activity can have an obvious adsorption effect, which can be used as an adsorbent [18]. Compared with ion exchange adsorbents, chelating agents have stronger binding capacity and higher selectivity. Therefore, the development of an adsorbent with chelating adsorption function is an important content of adsorbent research [19–21]. Because of the low production cost, high porosity, large specific surface area, and resistance to acids and alkalis and organic solvents, polystyrene resin-based chelating resins are the most widely studied and used metal ion adsorption materials [22]. In the process of heavy metal ion adsorption, the types of functional groups contained on the resin surface, the density of functional groups on the resin surface, and the interaction between functional groups and metal ions all affect the adsorption capacity and selectivity [23]. Therefore, choosing an appropriate surface modification method and increasing the density of functional groups on the resin surface is an important way to increase the adsorption capacity. Atom transfer radical polymerization (ATRP) is a new technology of controlled radical living polymerization, which can form a high-density polymer molecular brush structure on the surface of materials to achieve as many connections of functional group as possible on a limited area [24,25]. In recent years, many studies have been devoted to the preparation of high-performance adsorbents in combination with ATRP technology [26,27].

In this work, a novel sulfonic acid chelating resin was prepared by grafting 4-styrenesulfonic acid onto chloromethylated polystyrene using ATRP, and its adsorption performance on Pb(II), Cu(II), Cd(II), Cr(III) and Ni(II) in aqueous solution was investigated. A method for constructing high-density, polarity-controlled functional polymer molecular brushes on resin surfaces was established using ATRP technology. The effect of monomer grafting amount and polymer molecular brush polarity on adsorption capacity and selectivity was explored to provide theoretical guidance for the preparation of separation materials with high adsorption capacity and selectivity.

2. Experimental section

2.1. Materials

Chloromethylated polystyrene (Xi'an Lanxiao Science and Technology New Material Co., Ltd., China, with a chlorinity of 18% (mass fraction), a content of cross-linking agents of 6% (mass fraction)); 4-styrenesulfonic acid (CP, Shanghai Aladdin, China); cuprous bromide (CP, Tianjin Chemical Reagent Factory); 2,2′-bipyridine (CP, Tianjin Chemical Reagent Factory); All other chemicals were of analytical grade.

2.2. Preparation of poly(4-styrene sulfonic acid)-graft resins

2,2′-Bipyridyl (0.5 g), copper(I) bromide (0.05 g) and chloromethylated PS beads (5.0 g) were placed into a reaction vessel, and the mixture was de-oxygenated by repeated vacuumizing. High-purity nitrogen was introduced into the tube after each evacuation stage. Then, 4-styrenesulfonic acid (0.50 g) in 50 mL DMF previously de-oxygenated by three cycles of freeze–vacuum–thaw was added into the tube using a syringe under a nitrogen atmosphere. The reaction was performed at 65°C under stirring and a nitrogen atmosphere. The resulting poly(4-styrene sulfonic acid)-grafting PS resins (PSS-g-PS) were removed from the reaction solution after the desired reaction time and immersed in 60 mL of methanol-0.2 mol·L^{-1} Na_2EDTA solution (1:1, v/v) for 10 h to remove copper ions and then washed with water and methanol separately. The products were finally dried in vacuum oven at 35°C.

Polymerization time was used as an independent variable to control the grafting degree (DG) of 4-styrenesulfonic acid on the chloromethylated PS resin. DG was measured by the increase in the mass percentage of PSS-g-PS resins as described by Eq. (1).

$$\mathrm{GD}(\%) = \frac{W_a - W_b}{W_b} \times 100\% \tag{1}$$

where W_a and W_b are the weight of chloromethylated PS before and after grafting, respectively.

2.3. Characterization of adsorbents

Chemical composition information about the surface of the chloromethylated PS, and PSS-g-PS resins was analyzed using TM3000 Scanning Electron Microscope (Hitachi, Ltd., Japan), SwiftED3000 Energy Spectrometer (Hitachi, Ltd., Japan), Tensor 27 FTIR Spectrophotometer (Bruker Company, Germany), X-ray photoelectron spectroscopy (XPS, PE, PHI-5400, USA), Microelectrophoresis (JS94H, Shanghai Zhong Chen Digital Technology Equipment Co., Ltd., China).

2.4. Batch adsorption experiment

To study the adsorption properties and the factors effecting adsorption, batch adsorption experiments were carried out by using aqueous heavy metal ion solution. The experiments were carried out with different concentrations (50~1,000 mg·L^{-1}) of heavy metal ion solution, at different temperatures (25°C, 35°C and 45°C) and at different pH (1~7). Aliquots of 1.00 mL solution were taken at different time intervals. 0.1 g of PSS-g-PS beads was added into 100.00 mL of operational solution and then shaken on a shaker for 12 h. The beads were removed by filtration, and the filtrates were collected to measure the final ion concentration by atomic absorption spectrophotometry (AAS). Each experiment was conducted three times to ensure the accuracy of the experimental results. The adsorption capacity at equilibrium (Q_e, expressed in mmol·g^{-1}) was estimated from Eq. (2):

$$Q_e = \frac{V(C_0 - C_e)}{m} \tag{2}$$

where V is the volume of the solution (L), C_0 and C_e are the initial and equilibrium concentrations of metal ions (mg·L^{-1}), respectively, and m is the weight of the used resin (g).

2.5. Recycling experiments

The Pb(II), Cu(II), Cd(II), Cr(III) and Ni(II)-loaded resins were regenerated with 1.0 mol·L^{-1} HCl solution and then collected by filtration, washed with distilled water, and reused in the next cycle of adsorption experiments.

3. Results and discussion

3.1. Preparation of PSS-g-PS resins

The synthetic route in Fig. 1 was selected to prepare PSS-g-PS resin. PSS was grafted onto the surface of chloromethylated PS beads by surface-initiated atom transfer radical polymerization (SI-ATRP). ATRP is based on simple organic halide groups as the initiators in the polymerization reaction. Earlier studies have indicated that benzyl chloride is an effective initiator for SI-ATRP from a variety of substrates. Chloromethylated PS resin itself contains many benzyl chloride initiation sites and was directly used in this study. In SI-ATRP, two major variables are often used to control the degree of grafting, that is, the concentration of the monomer and the reaction time. Here, a series of PSS-g-PS resins with different DG values were prepared by adjusting the reaction time. The plot of DG vs. reaction time is presented in Fig. 2. As observed from this figure, DG displayed a linear increase with the increasing polymerization time within 10 h, indicating the living/controlled feature of SI-ATRP of 4-styrene sulfonic acid on chloromethylated PS beads. At 10 h, DG was up to 76%. However, when the grafting time was further extended, the growth rate slowed down gradually, and thus, DG displayed a deviation from the predicted linearity. The phenomenon was similar to results reported previously. The reason may possibly be attributed to the termination reaction in the process of SI-ATRP.

The relationship between DG and the adsorption capacity was also investigated, and the adsorption capacity of Pb(II), Cu(II), Cd(II), Cr(III) and Ni(II) on the PSS-g-PS resins prepared at different ATRP times is shown in Fig. 2. It can be seen that the adsorption capacity increased linearly with increasing ATRP time within 12 h, which was positively related to the amount of the grafted PSS on the resins. After 12 h, the increase in adsorption capacity slowed down, and this was related to the slower increase rate in DG. In terms of high capacity and short polymerization time, the ATRP time was maintained at 12 h in the following experiments.

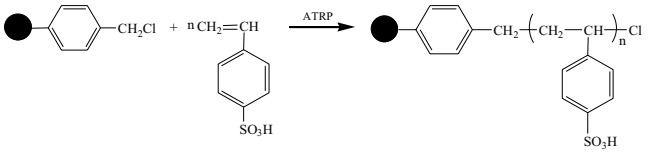

Fig. 1. Synthetic route for the preparation of PSS-g-PS resin.

3.2. Characterization of adsorbents

3.2.1. Analysis of scanning electron microscopy

The changes in surface morphology of chloromethylated PS, PSS-g-PS and PSS-g-PS loaded Pb(II) were studied by scanning electron microscopy (SEM). As seen in Fig. 3a and b, the surface morphology of the modified resin changed significantly, and the surface of the PSS-g-PS resin became smooth and regular compared with the unmodified chloromethylated PS resin. It may be due to the modification of PSS on the surface of chloromethylated PS resin by ATRP technique, which covered the surface with a high-density polymer molecular brush and partially blocked the pores of the original resin, thus the surface of the modified resin was smooth. After adsorption, the surface morphology of PSS-g-PS loaded Pb(II) changed significantly with a smooth and uniform surface, indicating that the metal ions

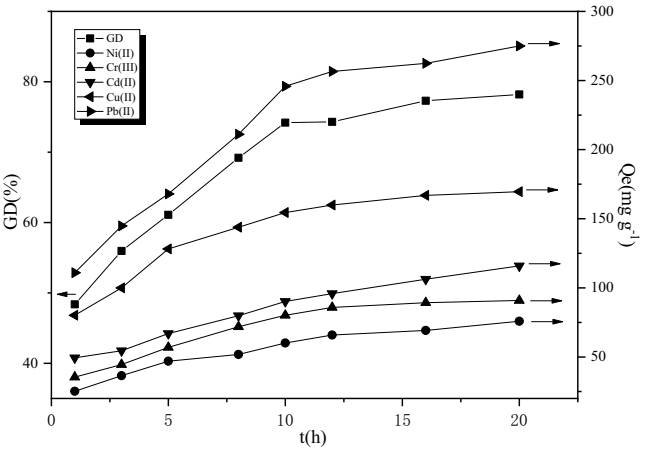

Fig. 2. Effects of the ATRP time on the grafting degree and adsorption capacity.

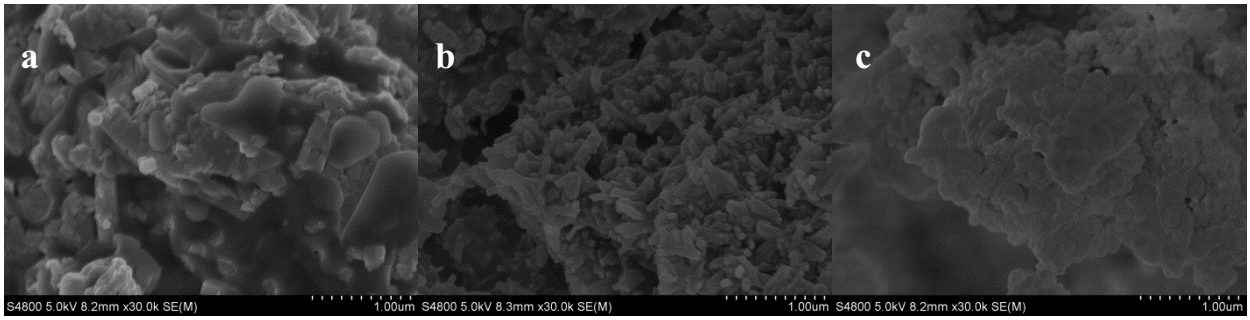

Fig. 3. Scanning electron microscopy of (a) chloromethylated PS, (b) PSS-g-PS and (c) PSS-g-PS loaded Pb(II).

occupied the pore channels of the resin, thus achieving the adsorption effect.

3.2.2. Analysis of energy-dispersive X-ray spectroscopy

The elemental compositions of chloromethylated PS, PSS-g-PS and PSS-g-PS loaded Pb(II) were obtained by energy-dispersive X-ray spectroscopy. The results are shown in Table 1.

As known from Table 1, the presence of S and O elements after modification indicated that PSS was successfully grafted onto the surface of chloromethylated PS. By comparing the elemental composition of PSS-g-PS and PSS-g-PS loaded Pb(II), it can be seen that Pb(II) is adsorbed on PSS-g-PS, which proves that PSS-g-PS is an effective metal ion adsorption material that can be used to adsorb and remove harmful metal ions from water bodies, thus achieving the purpose of metal enrichment and water purification.

3.2.3. Analysis of Fourier-transform infrared spectroscopy

Structural characterization of chloromethylated PS, PSS-g-PS and PSS-g-PS loaded Pb(II) were performed by Fourier-transform infrared spectroscopy (FTIR) technique, and their spectra have been given in Fig. 4. As seen from Fig. 4a, the characteristic peaks at 2,924 and 1,450 cm^{-1} can be assigned to C–H stretching and skeleton vibration of the aromatic ring, respectively. The peaks at 759 and 698 cm^{-1} are due to C–Cl stretching in $–CH_2Cl$ group. The newly added absorption peak at 987 and 1,126 cm^{-1} in Fig. 4b are caused by the stretching vibration of the O=S=O group in PSS-g-PS resin, the peaks at 3,460 cm^{-1} is due to –OH stretching in $–SO_3H$ group, indicating that the sulfonic acid group has been successfully grafted to the surface of PS resin via ATRP. After the adsorption of Pb(II) (Fig. 4c), the absorption peaks of S=O did not change much and the stretching vibration peaks of –OH weakened, indicating that –OH was involved in the chelation of adsorbed metal ions.

3.2.4. Analysis of X-ray photoelectron spectroscopy

By analyzing the wide-scan X-ray photoelectron (XPS) spectrum (Fig. 5), we could easily find the chemical change in the structure of the modified resins. For chloromethylated PS beads, there was no sulfur and oxygen emission. After SI-ATRP, the S 2p and O1s peak at approximately 169 and 532 eV, respectively was observed in the PSS-g-PS resin, indicating that sulfonic acid groups were successfully introduced onto the resin surface.

To obtain more detailed information about the change in the composition of the surface of PSS-g-PS resin, the peak components of the C 1s peak in the XPS spectra were further analyzed by the core-level spectrum (Fig. 6). The C 1s core-level of the PSS-g-PS resin could be curve-fitted into three peak components. In comparison with PS, the peak with a binding energy of 285.8eV was added, which could be assigned to C–S species. Collectively, the FTIR and XPS results confirmed the successful grafting of poly(4-styrene sulfonic acid) on the surface of the resin.

Table 1
Element composition of chloromethylated PS, PSS-g-PS and PSS-g-PS loaded Pb(II)

Element	Weight percentage (%)		
	Chloromethylated PS	PSS-g-PS	PSS-g-PS loaded Pb(II)
C	77.56	70.45	65.63
Cl	20.32	14.46	11.25
O	–	8.96	6.78
S	–	4.89	3.98
Pb	–	–	10.82

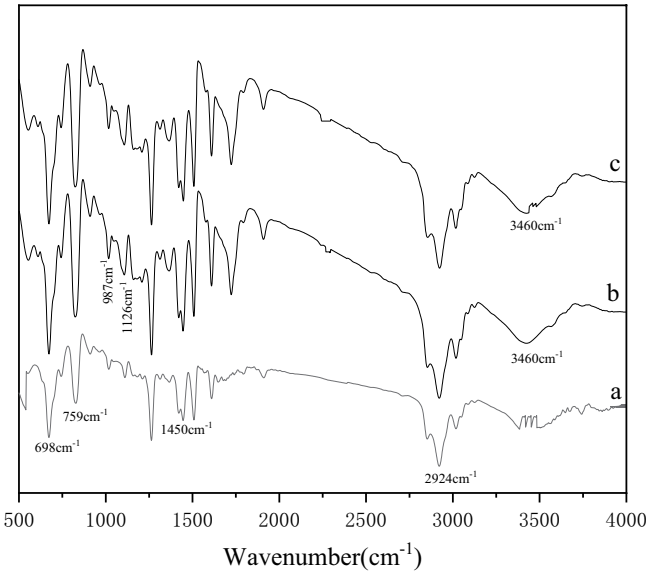

Fig. 4. Fourier-transform infrared spectroscopy of (a) chloromethylated PS, (b) PSS-g-PS and (c) PSS-g-PS loaded Pb(II).

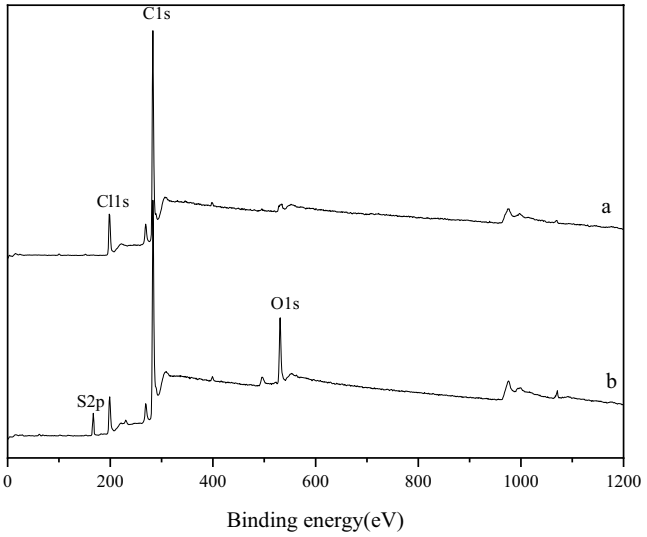

Fig. 5. X-ray photoelectron spectroscopy wide scan of (a) chloromethylated PS, (b) PSS-g-PS.

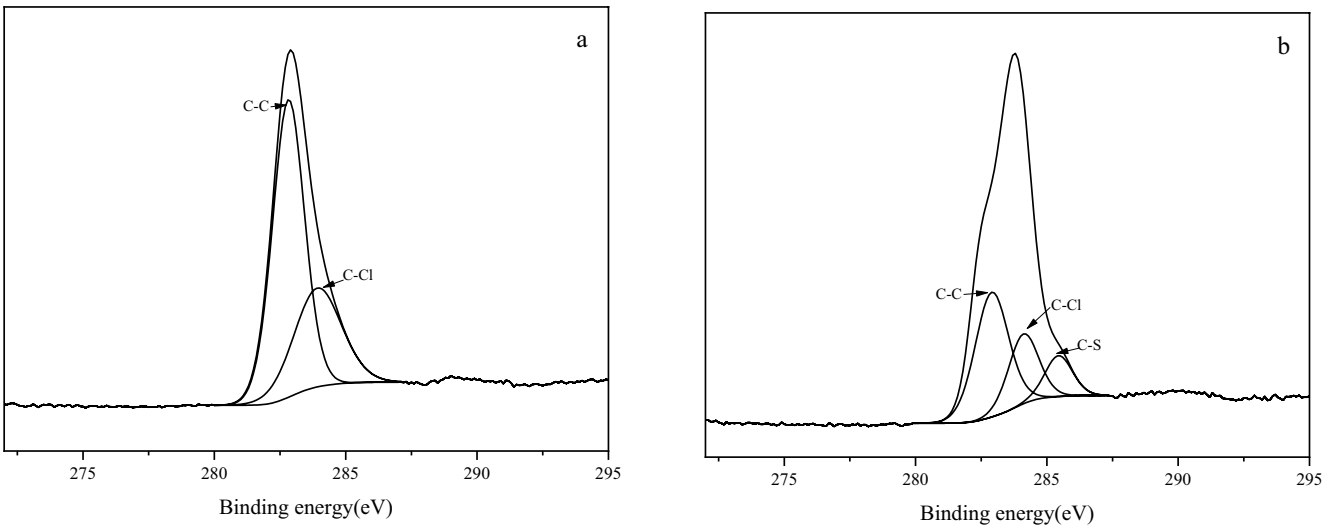

Fig. 6. C 1s core-level spectra of chloromethylated PS (a) and PSS-g-PS (b).

3.2.5. Analysis of zeta potential

Zeta potential is the potential generated by the surface charge of colloidal particles dispersed in solution. Various mechanisms such as dissociation of functional groups on the surface of the particles, adsorption of the surfactants and ion adsorption make the surface charged. A large number of polar groups exist on the surface of PSS-g-PS, and when it is dispersed in solution, a certain amount of ions can be adsorbed on the surface of PSS-g-PS to form an electric double layer, thereby generating a zeta potential.

The pH zeta potential curves of PSS-g-PS is presented in Fig. 7. As shown in Fig. 7, when pH value increases from 2.0 to 5.0, the negative charge of PSS-g-PS increase from 0.75 to –17.9. Increasing the negative charge on the surface, the more conducive to attract positively charged metal ions and can be conducive to adsorption of heavy metal ions.

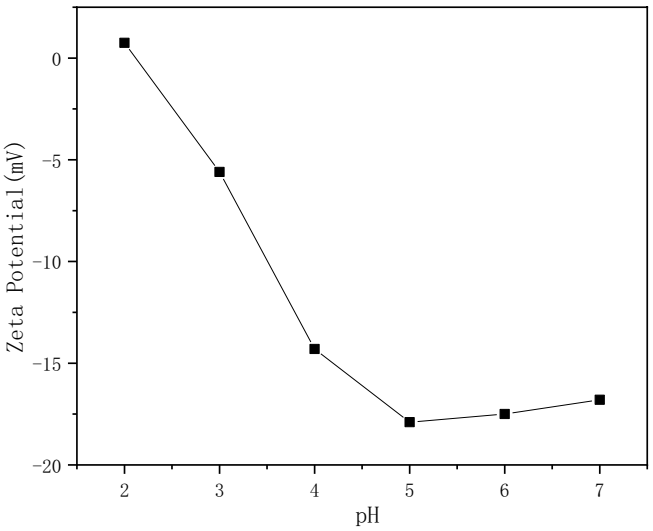

Fig. 7. Variation of zeta potentials of PSS-g-PS as a function of pH values.

3.3. Adsorption of metal ions from aqueous solutions

3.3.1. Effect of pH on adsorption

pH has a direct effect on the adsorption sites of metal ions on the adsorbent surface and the chemical morphology of metal ions. As for most adsorption processes, pH can influence not only the characteristics of the composition of the surface structures of polymeric adsorbents but also the form of existence of heavy metal ions in solution. The adsorption of metal ions was examined at different pH values, as shown in Fig. 8. An abrupt increase in the adsorption capacity was observed when the pH increased from 1.0 to 4.0, and the plateau values were approximately 5.0 for all cases. At lower pH, the concentration of H_3O^+ in the solution is high and the active sites of the adsorbent were less available for metal ions due to greater repulsive forces. Moreover, a great excess of hydrogen ions could compete with metal ions and further lead to the decrease in metal uptake. As the pH rose to pH > 4, the competition of H^+ become weaker and more binding sites are occupied by metal ions, the strong adsorption of the adsorbent to metal ions occurred. The low adsorption capacity at lower pH indicated that the resin could be regenerated in acidic solution. The maximum adsorption capacity for Pb(II), Cu(II), Cd(II), Cr(III) and Ni(II) was found at pH 4.0~7.0. To exclude the possibility of the hydrolysis of metal ions, pH 5.0 was selected as the optimum pH for the subsequent adsorption experiments. This result is consistent with the variation of zeta potentials of PSS-g-PS as a function of pH values.

3.3.2. Effect of contact time on adsorption

Fig. 8 indicates the effect of contact time on the heavy metal ion adsorption. It can be seen from Fig. 9 that the adsorption capacity of heavy metal ions increased rapidly within initial 2h, and then gradually increased until the adsorption process reached equilibrium. The reason for

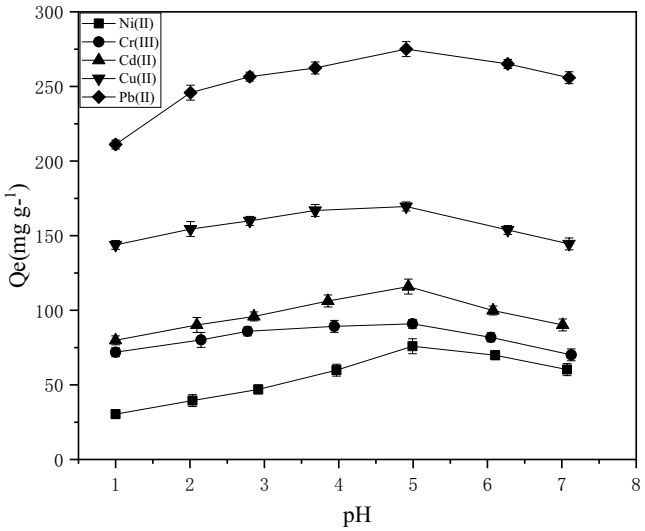

Fig. 8. Effect of pH on the adsorption of PSS-g-PS resin for Pb(II), Cu(II), Cd(II), Cr(III) and Ni(II) (initial concentration: 200 mg·L^{-1}; 25°C; adsorbent dose: 0.2 g).

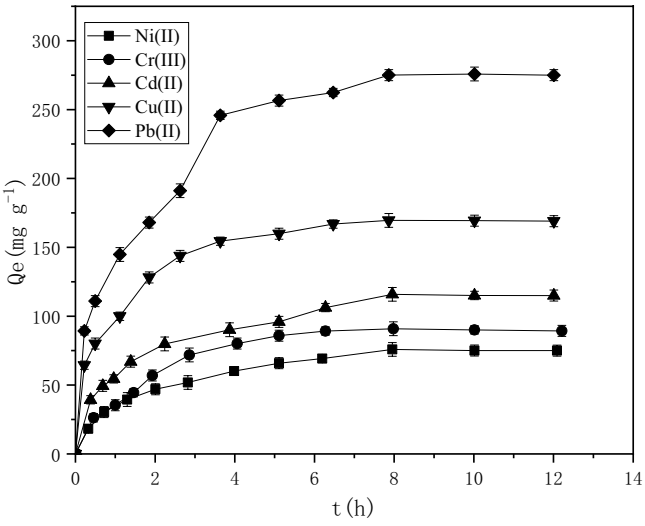

Fig. 9. Adsorption kinetics of PSS-g-PS resin for Pb(II), Cu(II), Cd(II), Cr(III) and Ni(II) at 25°C (initial concentration: 200 mg·L^{-1}; pH 5.0; adsorbent dose: 0.2 g).

the rapid increase of adsorption capacity may be that there were many active sites on the surface of PSS-g-PS resin. At the initial stage of adsorption, metal ions could approach more active sites on the surface of PSS-g-PS resin. With the progress of the adsorption process, there was not enough active site on the surface of PSS-g-PS resin to combine with heavy metal ions, which leading to the slow change of adsorption capacity until the adsorption equilibrium was reached.

3.3.3. Effect of the initial concentration of metal ions

Fig. 10 illustrates the result of sorption capacity for heavy metal ions as the variety of the initial metal ion concentration. It was observed that more and more heavy metal

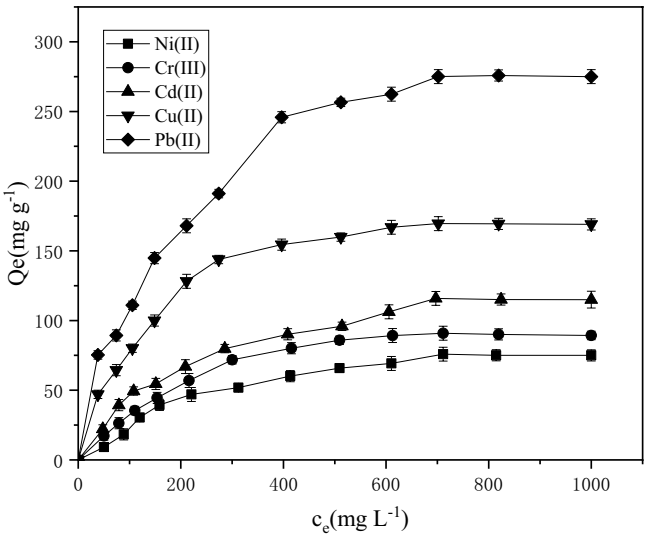

Fig. 10. Adsorption isotherms of PSS-g-PS resin for Pb(II), Cu(II), Cd(II), Cr(III) and Ni(II) at 25°C (pH 5.0; contact time: 12 h; adsorbent dose: 0.2 g).

ions were adsorbed with the increase of initial concentration. The maximum adsorption capacity reached 275 mg·g^{-1} for Pb(II), 169 mg·g^{-1} for Cu(II), 115 mg·g^{-1} for Cd(II), 90.8 mg·g^{-1} for Cr(III) and 75 mg·g^{-1} for Ni(II), respectively. After reaching the highest points, it gradually decreased. It may be that with the increase of initial metal ion concentration, heavy metal ions had specific advantages in the process of competing for active sites, and more metal ions combine with active sites. At the same time, the increase in mass transfer rate was attributed to the increase in the driving force of the ions, resulting in high adsorption capacity. However, the adsorption capacity decreased with the increase of the initial heavy ion concentration, subsequently. It might be attributed that a large number of active sites were occupied, resulting in insufficient adsorption sites. Thus, a low adsorption capacity was obtained.

3.4. Analysis of adsorption isotherms

Two theoretical isotherm models, the Langmuir (3) and Freundlich (4) models, are often used to describe and analyze the adsorption isotherm. The Langmuir model is based on the assumption of surface homogeneity such as equally available adsorption, monolayer surface coverage, and no interaction between adsorbed species, whereas the Freundlich model assumes that the adsorption occurs on a heterogeneous surface.

$$\frac{C_e}{Q_e} = \frac{C_e}{Q_0} + \frac{1}{Q_0 b} \tag{3}$$

$$\ln Q_e = \ln K_F + \frac{1}{n} \ln C_e \tag{4}$$

where Q_e is the adsorption capacity, mg·g^{-1}; C_e is the equilibrium concentration of metal ions, mg·L^{-1}; Q_0 is the saturated adsorption capacity, mg·g^{-1}; K_F is an empirical

parameter; n is the Freundlich constant; and K_F is the binding energy constant reflecting the affinity of the adsorbents to metal ions. b is the Langmuir adsorption constant, and its relation of the adsorption equilibrium constant between the solid and liquid (aqueous solution) has the following relation as follows:

$$b = \left(K_c - 1\right)\frac{M}{\rho} \tag{5}$$

where M and ρ are the molar mass (g·mol^{-1}) and density (g·mol^{-1}) of the solvent, respectively.

The adsorption isotherms were fitted with the Langmuir and Freundlich equations, respectively, and the results are shown in Fig. 11. The values of the parameters of isotherm models at 298 K are given in Table 2. According to the fitting curves from two different isotherm models and the correlation coefficients (R^2), the adsorption capacities from the Langmuir isotherm model had highest correlation coefficients than Freundlich isotherm models. Thus, it was believed the five heavy metal ions of adsorption process was carried out on the homogeneous surface. In addition, the actual value of metal ions adsorbed by the PSS-g-PS resins was closer to the theoretical value of the Langmuir isotherm model.

3.5. Analysis of adsorption kinetics

Three different kinetic models: Lagergren's pseudo-first-order kinetic model (6), pseudo-second-order kinetic model (7) and intraparticle diffusion model (8) proposed by Weber and Morris were used to illustrate the kinetic process.

$$\log\left(Q_e - Q_t\right) = \log Q_e + \frac{k_{ads}}{2.303}t \tag{6}$$

$$\frac{t}{Q_t} = \frac{1}{kQ_e^2} + \frac{1}{Q_e}t \tag{7}$$

$$Q_t = k_{id}t^{0.5} + C \tag{8}$$

where t is the adsorption time (min); k the adsorption rate constant (h^{-1}); K_{ads} is the Lagergren rate constant (h^{-1}) of the adsorption; K_{id} is the intraparticle diffusion rate constant (mg·g^{-1}/h$^{0.5}$), C is the intercept value, and Q_t and Q_e are the adsorption amount at given time t and equilibrium time, respectively.

If Q_t vs. $t^{1/2}$ is linear and the line passes through the origin, intraparticle diffusion is included in the sorption process. Also, C gives an indication about the thickness of boundary layer.

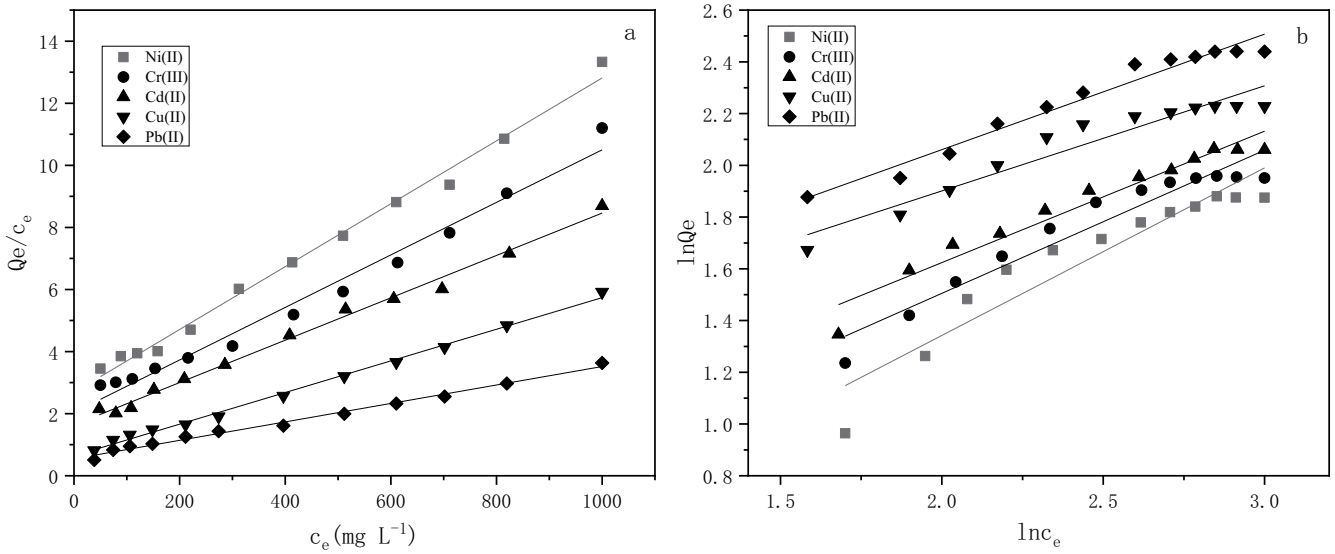

Fig. 11. Fitting curve of the (a) Langmuir and (b) Freundlich isotherm model.

Table 2
Langmuir and Freundlich constants for the adsorption of Pb(II), Cu(II), Cd(II), Cr(III) and Ni(II) on PSS-g-PS resins at 25°C

Metal ions	Experimentally determined	Langmuir constants				Freundlich constants		
	Q_e (mg·g^{-1})	Q_0 (mg·g^{-1})	b	K_C	R_L^2	K_F	$1/n$	R_F^2
Pb(II)	275	336.7	2.35	131.6	0.99023	1.048	0.6478	0.9634
Cu(II)	169	196.1	1.97	110.4	0.99523	1.490	0.5533	0.92134
Cd(II)	115	146.4	1.58	88.8	0.99187	1.837	0.5081	0.9462
Cr(III)	90.8	118.2	1.39	78.2	0.97956	2.969	0.4064	0.92439
Ni(II)	75	98.7	1.15	64.9	0.99159	3.213	0.4466	0.88614

To understand the adsorption nature of heavy metal ions on PSS-g-PS resins, the curves obtained using linearized equations of the pseudo-first-order and pseudo-second-order model are shown in Fig. 12, respectively.

Kinetic parameters determined from pseudo-first-order [Eq. (6)], pseudo-second-order [Eq. (7)] and intraparticle diffusion [Eq. (8)] models are presented in Table 3. It can be seen that the pseudo-second kinetic model provides a good correlation for the adsorption of heavy metal ions on the PSS-g-PS resins (R^2 values). Furthermore, the Q_e values calculated by the pseudo-second-order model are close to the experimentally determined Q_e values. That is, in this adsorption process, the pseudo-second-order kinetic model accurately describes the kinetic behavior of heavy metal ions on the PSS-g-PS resins. In order to determine the importance of diffusion in the adsorption process, the graph drawn between the amount of adsorbed metal (Q) and the square root of time ($t^{1/2}$) is given in Fig. 12 and multi-linear stages were observed.

According to Weber and Morris, an adsorption process is divided into three steps: (1) diffusion of the adsorbate from the solution to the surface of the adsorbent; (2) internal diffusion process, usually determined by the pore size of the adsorbent; (3) adsorption of the adsorbate with the surface active sites in the adsorbent.

According to the equation (8), if the curve gives a straight line, internal diffusion can be accepted as the only rate limiting step, but multiple linearities are formed, indicating that two or more stages are involved in metal ion adsorption. As shown in Fig. 13, the adsorption process is divided into three stages: (1) rapid transport of metal ions from solution to the surface of the resin (2) gradual adsorption stage, where intraparticle diffusion is the rate limiting step, and (3) final equilibrium stage, intraparticle diffusion begins to slow down because the concentration of metal ions in the solution is very low and the number of available adsorption sites is small.

From the above analysis, it can be seen that intraparticle diffusion was not the only rate-controlling step, indicating that the adsorption process involved several single kinetic stages.

3.6. Analysis of adsorption thermodynamics

The adsorption capacity of heavy metal ions on the PSS-g-PS resins were increased with the increasing of

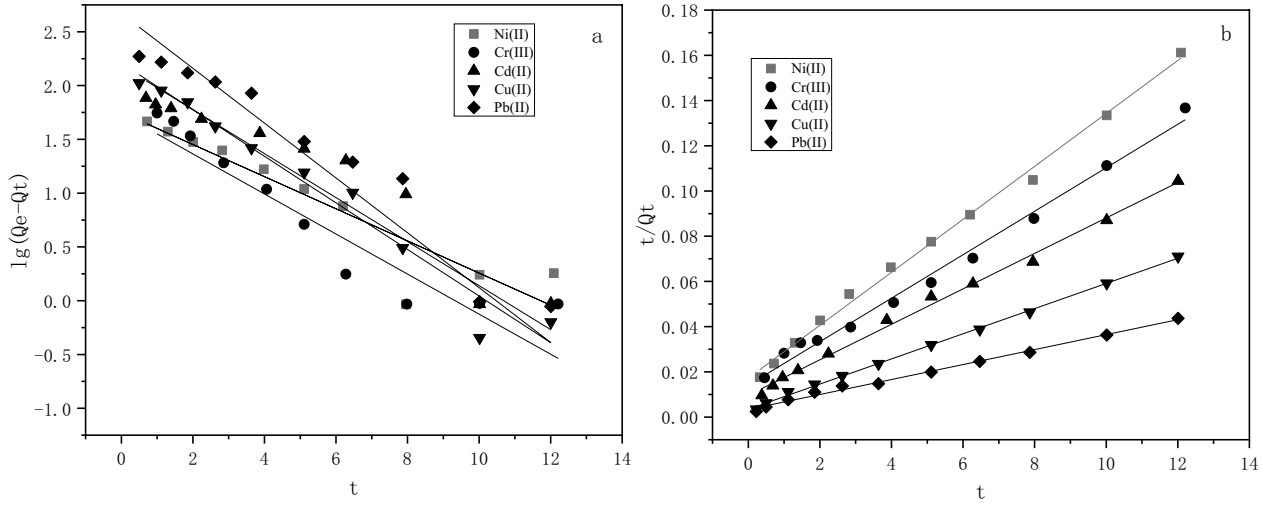

Fig. 12. Pseudo-first-order (a) and pseudo-second-order (b) plots.

Table 3
Related parameters of kinetic model

Equations	Parameter	Pb(II)	Cu(II)	Cd(II)	Cr(III)	Ni(II)
Experimentally determined	Q_e (mg·g^{-1})	275	169	115	90.8	75
	Q_e (mg·g^{-1})	205.3	158.5	96.5	54.6	56.4
Pseudo-first-order kinetic equation	K_{ads} (h^{-1})	0.587	0.50	0.461	0.428	0.342
	R^2	0.925	0.960	0.754	0.639	0.846
	Q_e (mg·g^{-1})	302.1	179.9	127.6	104.1	85.4
Pseudo-second-order kinetics	k (g·mg^{-1}·h^{-1})	0.0032	0.0089	0.0064	0.0065	0.0080
	R^2	0.994	0.999	0.995	0.991	0.996
	K_{id} (mg·g^{-1}·h$^{-1/2}$)	0.0615	0.0497	0.0393	0.0208	0.0156
Intraparticle diffusion equation	C (mg·g^{-1})	93.5	78.5	35.2	28.1	20.1
	R^2	0.924	0.848	0.945	0.839	0.905

temperature, but the increasement was not significant in the temperature range investigated (Fig. 14), which confirmed that the adsorption was an endothermic process.

The thermodynamic parameters provide in-depth information on inherent energetic changes that are associated with adsorption, including free energy change (ΔG), enthalpy change (ΔH) and entropy change (ΔS), which can be respectively estimated using the following equations:

$$\Delta G = -RT\ln K_c \tag{9}$$

$$\ln K_c = \frac{-\Delta H}{RT} + \frac{\Delta S}{R} \tag{10}$$

where R is the universal gas constant (8.314 J·mol^{-1}·K^{-1}), T the absolute temperature (K), and K_C the adsorption equilibrium constant, which was obtained from the Langmuir isotherm at different temperatures.

The values of thermodynamic parameters are calculated and summarized in Table 4. The thermodynamic parameters of heavy metal ions adsorption onto PSS-g-PS resins indicated that the adsorption was spontaneous and endothermic owing to the negative value of ΔG and positive value of ΔH. The observed increase in the negativity of ΔG with increasing temperature suggested that the favorability of adsorption increases with temperature. The positive value of ΔS confirmed an increased disorder at the solid–liquid interface during the adsorption process.

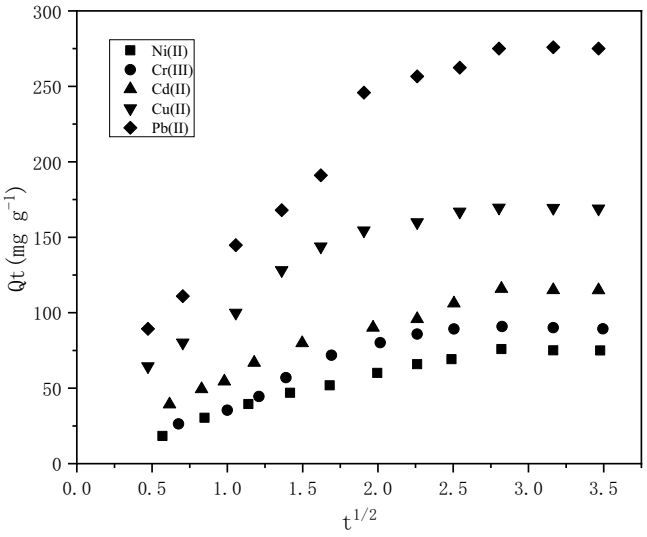

Fig. 13. Intraparticle diffusion model.

3.7. Regeneration of PSS-g-PS

Considering long-term economy and potential practical application, adsorption of PSS-g-PS resins should owe excellent features with recyclability and reusability. The result is depicted in Fig. 15. After 10 cycles of adsorption–desorption, there was still more than 95.6% for Pb(II), 94.1% for Cu(II), 93.1% for Cd(II), 92.2% for Cr(III) and 90.6% for Ni(II) of adsorption capacity, indicating that the adsorbent of PSS-g-PS resins had a good reusable performance. The excellent performance offers potential for the treatment of pollution in the water environment by the adsorbent.

3.8. Comparison with other adsorbents

There are many adsorbents designed for different metal ions in the reference, from which the representative adsorbents that can adsorb Pb(II), Cu(II), Cd(II), Cr(III)

Table 4
Thermodynamic parameters Estimated for adsorption of Pb(II), Cu(II), Cd(II), Cr(III) and Ni(II) on PSS-g-PS resins

Metal ions	ΔH (kJ·mol^{-1})	ΔS (J·mol^{-1}·K^{-1})	ΔG (kJ·mol^{-1})		
			25°C	35°C	45°C
Pb(II)	53.03	218.50	–12.09	–14.32	–16.37
Cu(II)	30.63	141.80	–11.65	–13.15	–14.32
Cd(II)	20.12	104.80	–11.12	–12.20	–13.15
Cr(III)	5.74	55.50	–10.80	–11.35	–11.92
Ni(II)	0.46	36.30	–10.34	–10.65	–11.17

Table 5
Adsorption capability of various adsorbents for Pb(II), Cu(II), Cd(II), Cr(III) and Ni(II)

Adsorbent	Q_e (mg·g^{-1})					References
	Pb(II)	Cu(II)	Cd(II)	Cr(III)	Ni(II)	
A novel, mesoporous, and industrial waste clay mixture	–	8.63	–	–	–	[28]
Schleichera oleosa bark	69.44	–	–	–	–	[29]
Magnetic responsive mesoporous alginate/β-cyclodextrin polymer beads	21.09	15.54	2.47	–	2.68	[30]
PVB-PVA blend polymer nanocomposite	111.23	172.54	112.89	–	–	[31]
C-phenylcalix[4]pyrogallolarene material	60.97	8.14	–	14.31	16.16	[32]
Ball clay	–	–	27.17	–	–	[33]
Seeds of *Artemisia absinthium*	–	–	–	46.99	–	[34]
Sulfonated covalent organic frameworks (COF@SO_3H)	–	–	81.97	105.26	–	[35]
Bioadsorbent of sodium alginate grafted polyacrylamide/graphene oxide hydrogel	240.69	68.76	–	–	–	[36]
PSS-g-PS resins	275	169	115	90.8	75	This work

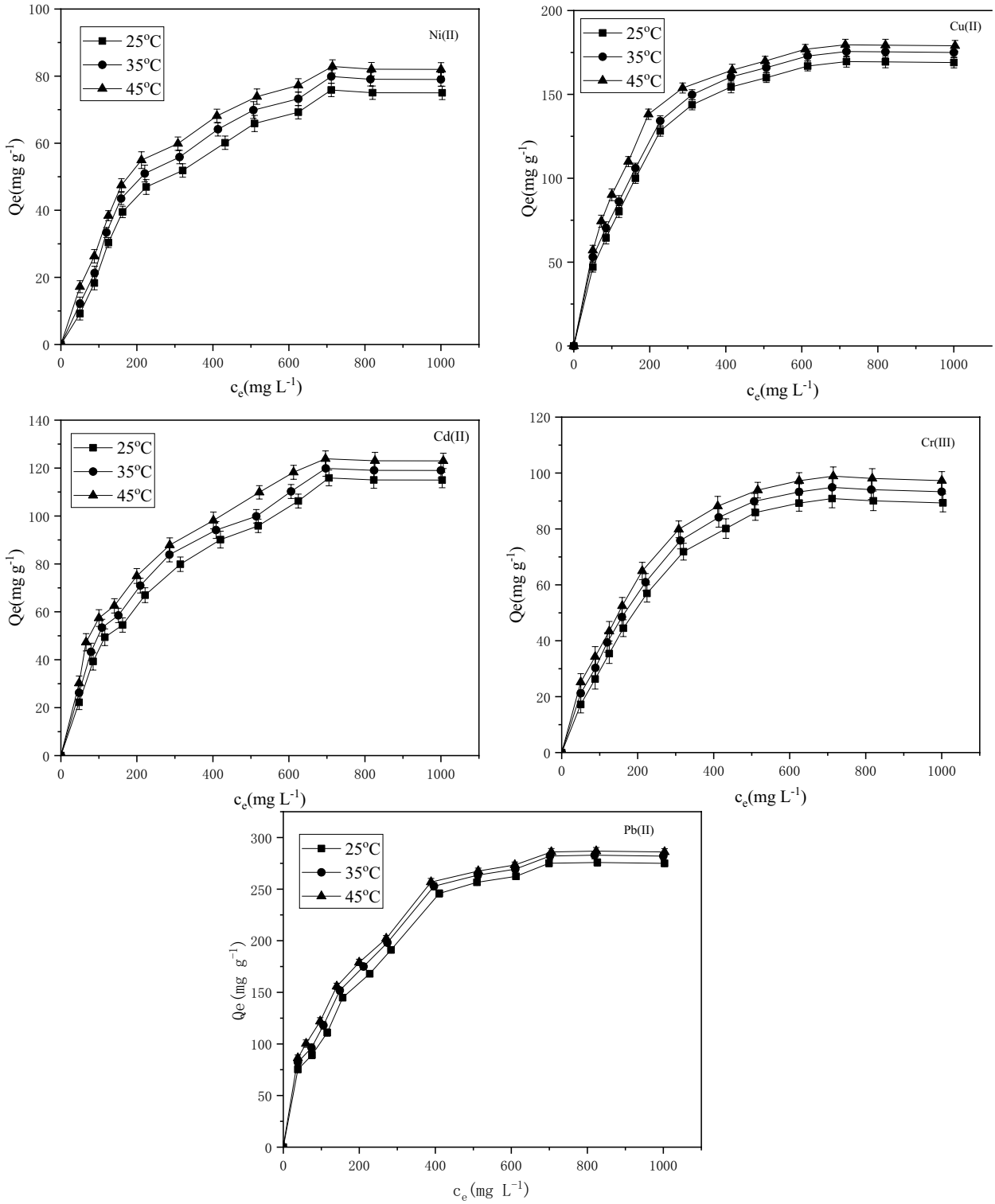

Fig. 14. Adsorption isotherms of PSS-g-PS resin for Pb(II), Cu(II), Cd(II), Cr(III) and Ni(II) at different temperature (pH 5.0; contact time: 12 h; adsorbent dose: 0.2 g).

and Ni(II) ions were chosen for comparison with PSS-g-PS resins. The selected adsorbents include synthesis resins, functionalized active carbon and modified waste products. As shown in Table 5, PSS-g-PS resins possessed the advantage mainly on the adsorption capacities. PSS-g-PS resins had much higher adsorption capacities for the three metal ions than the carbon or waste products. Compared with synthesized resin, the adsorption capacity

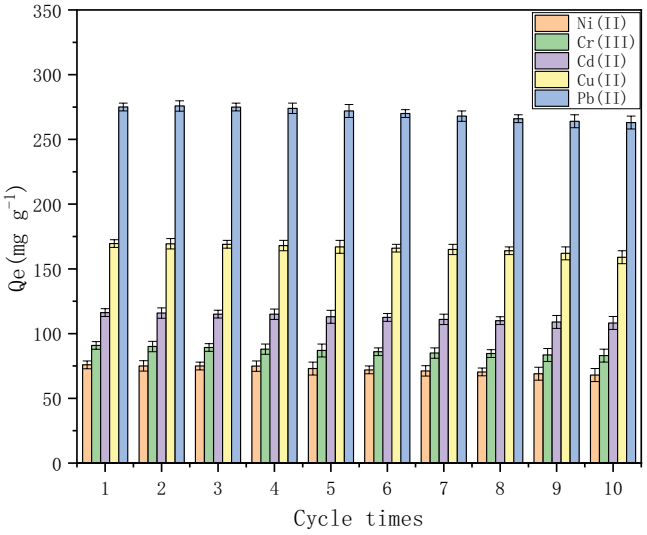

Fig. 15. Adsorption capacity after ten adsorption–desorption cycles.

of PSS-g-PS resins was much higher than some commercial cation exchange resins. Higher adsorption capacities can produce higher productivity for water treatment. Therefore, the resin should be of value in water treatment on the basis of sustainability principles.

4. Conclusion

In this work, a novel poly(4-styrene sulfonic acid)-graft resin (PSS-g-PS) with high capacity was prepared by SI-ATRP of poly(4-styrene sulfonic acid) (PSS) The graft amount of PSS from the chloromethylated PS resin was found to increase linearly with the polymerization time, indicating the living/controlled character of SI-ATRP. SEM, FTIR and XPS confirmed the successful grafting of PSS and the formation of PSS-g-PS polymer onto the surface of the resin.

Batch adsorption experiments show that the best adsorption is observed at a pH 5.0 for the five heavy metal ions. The adsorption isotherms and kinetics of five studied ions onto PSS-g-PS resins can be well described by the Langmuir isotherm model and the pseudo-second-order model, respectively. The obtained data indicated that the metal ions were adsorbed as a monolayer on the adsorbent surface, and the maximum adsorption capacities for Pb(II), Cu(II), Cd(II), Cr(III) and Ni(II) at 298 K are up to 275, 169, 115, 90.8 and 75 mg·g^{-1}, respectively. The thermodynamic parameters suggest that the adsorption of heavy metal ions onto PSS-g-PS resins is spontaneous. The adsorption–desorption cycles demonstrated that the resin was suitable for reuse in the removal of heavy metal ions.

Acknowledgement

This work was supported by "Cyanine Talent" of Xianyang Normal College (No. XSYQL201710), Innovative Entrepreneurship Training Program for College Students (No. 202310722055), Science and Technology Plan Project of Xianyang (No. L2022-XCZX-002), Shaanxi Province Science and Technology Plan Project of China (No. 2022GY-381).

References

[1] A.H.J. Ake, M. Hafidi, Y. Ouhdouch, L. EL Fels, Physico-chemical characterization and pollutant charge of industrial effluents from tanneries under semi-arid climate, Desal. Water Treat., 260 (2022) 148–160.
[2] Z.K. Lin, Y. Yang, Z.Z. Liang, L. Zeng, A. Zhang, Preparation of chitosan/calcium alginate/bentonite composite hydrogel and its heavy metal ions adsorption properties, Polymers, 13 (2021) 1891, doi: 10.3390/polym13111891.
[3] C.X. Shi, Y.Z. Li, X. Li, X.H. Zhao, X.T. Ma, X. Zhou, Y.M. Cui, S.M. Ma, W.L. Xu, C.G. Ren, Preparation of macroporous high adsorbent resin and its application for heavy metal ion removal, ChemistrySelect, 6 (2021) 9038–9045.
[4] M.R. Mahananda, S.K. Behera, B.P. Mohanty, S. Mishra, Adsorption efficiency of *Albizia lebbeck* (Indian siris) as bio-adsorbent for quantitative removal of lead metal ion from contaminated waters, Appl. Ecol. Environ. Sci., 9 (2021) 856–864.
[5] P. Rathore, R. Verma, Sorption capacity of toxic heavy metal Cr(VI) ion on bentonite clay from aqueous solution by kinetic and thermodynamic studies, Orient. J. Chem.: An Int. Res. J. Pure Appl. Chem., 37 (2021) 370512, doi: 10.13005/ojc/370512.
[6] Q.Q. Cai, B.C.Y. Lee, S.L. Ong, J.Y. Hu, Fluidized-bed Fenton technologies for recalcitrant industrial wastewater treatment–recent advances, challenges and perspective, Water Res., 190 (2021) 116692, doi: 10.1016/j.watres.2020.116692.
[7] A. Alharbi, A.M. Desouky, S. Bayoumi, A. Shahat, M.E.A. Ali, A hybrid polysulfone/mesoporous silica ultrafiltration membranes for industrial wastewater treatment, Desal. Water Treat., 252 (2022) 66–76.
[8] A. Lassoued, M. Ben Hassine, F. Karolak, B. Dkhil, S. Ammar, A. Gadri, Synthesis and magnetic characterization of spinel ferrites MFe_2O_4 (M = Ni, Co, Zn and Cu) via chemical co-precipitation method, J. Mater. Sci.: Mater. Electron., 28 (2017) 18857–18864.
[9] C.-Y. Tsai, Y.-L. Liu, Building up ion-conduction pathways in solid polymer electrolytes through surface and pore functionalization of PVDF porous membranes with ionic conductors, J. Membr. Sci., 651 (2022) 120456, doi: 10.1016/j.memsci.2022.120456.
[10] S.T. Han, W.Y. Li, H.L. Xi, R.S. Yuan, J.L. Long, C. Xu, Plasma-assisted in-situ preparation of graphene-Ag nanofiltration membranes for efficient removal of heavy metal ions, J. Hazard. Mater., 423 (2022) 127012, doi: 10.1016/j.jhazmat.2021.127012.
[11] S. Benalla, F.Z. Addar, M. Tahaikt, A. Elmidaoui, M. Taky, Heavy metals removal by ion-exchange resin: experimentation and optimization by custom designs, Desal. Water Treat., 262 (2022) 347–358.
[12] R.A.K. Rao, M. Kashifuddin, Adsorption properties of coriander seed powder (*Coriandrum sativum*): extraction and pre-concentration of Pb(II), Cu(II) and Zn(II) ions from aqueous solution, Adsorpt. Sci. Technol., 30 (2012) 127–146.
[13] H.Y. Sun, J. Zhan, L. Chen, Y.P. Zhao, Preparation of CTS/PAMAM/SA/Ca^{2+} hydrogel and its adsorption performance for heavy metal ions, Appl. Surf. Sci., 607 (2023) 155135, doi: 10.1016/j.apsusc.2022.155135.
[14] S. Kaviani, D.A. Tayurskii, O.V. Nedopekin, I. Piyanzina, DFT insight into Cd^{2+}, Hg^{2+}, Pb^{2+}, Sn^{2+}, As^{3+}, Sb^{3+}, and Cr^{3+} heavy metal ions adsorption onto surface of bowl-like B30 nanosheet, J. Mol. Liq., 365 (2022) 120131, doi: 10.1016/j.molliq.2022.120131.
[15] M. Abaszadeh, R. Hosseinzadeh, M. Tajbakhsh, S. Ghasemi, The synthesis of functionalized magnetic graphene oxide with 5-amino-1,10-phenanthroline and investigation of its dual application in C-N coupling reactions and adsorption of heavy metal ions, J. Mol. Struct., 1261 (2022) 132832, doi: 10.1016/j.molstruc.2022.132832.
[16] C.J. Feng, M. Huang, C.-P. Huang, Specific chemical adsorption of selected divalent heavy metal ions onto hydrous γ-Fe_2O_3-biochar from dilute aqueous solutions with pH as a master

variable, Chem. Eng. J., 451 (2023) 138921, doi: 10.1016/j.cej.2022.138921.
[17] G.Y. Duan, Z.F. Cao, H. Zhong, X. Ma, S. Wang, Highly efficient poly(6-acryloylamino-N-hydroxyhexanamide) resin for adsorption of heavy metal ions, J. Environ. Manage., 308 (2022) 114631, doi: 10.1016/j.jenvman.2022.114631.
[18] H.R. Wu, G. Lin, C.C. Liu, S.Y. Chu, C. Mo, X.B. Liu, Progress and challenges in molecularly imprinted polymers for adsorption of heavy metal ions from wastewater, Trends Environ. Anal. Chem., 36 (2022) e00178, doi: 10.1016/j.teac.2022.e00178.
[19] X.C. Zeng, G.H. Zhang, J.F. Zhu, Selective adsorption of heavy metals from water by a hyper-branched magnetic composite material: characterization, performance, and mechanism, J. Environ. Manage., 314 (2022) 114979, doi: 10.1016/j.jenvman.2022.114979.
[20] B.J. Gao, Y.C. Gao, Y.B. Li, Preparation and chelation adsorption property of composite chelating material poly(amidoxime)/SiO_2 towards heavy metal ions, Chem. Eng. J., 158 (2010) 542–549.
[21] A. Mary, L. Bradley, M. Ray, Z. Eugene, V. Aleksey, Adsorption of heavy metal ions on mesoporous silica-modified montmorillonite containing a grafted chelate ligand, Appl. Clay Sci., 59–60 (2012) 115–120.
[22] Y.N. Chen, M.F. He, C.Z. Wang, Y.M. Wei, A novel polyvinyltetrazole-grafted resin with high capacity for adsorption of Pb(II), Cu(II) and Cr(III) ions from aqueous solutions, J. Mater. Chem. A, 2 (2014) 10444–10453.
[23] Y.P. Wen, Z.F. Xie, S.S. Xue, J. Long, W. Shi, Y.C. Liu, Preparation of novel polymethacryloyl hydrazone modified sodium alginate porous adsorbent with good stability and selective adsorption capacity towards metal ions, Sep. Purif. Technol., 303 (2022) 122184, doi: 10.1016/j.seppur.2022.122184.
[24] Z. Mohamadnia, P. Tari, S. Amani, Preparation of smart brush-type cation-exchange adsorbents grafted nanosurface via SI-ATRP for dye removal, Colloids Surf., A, 624 (2021) 126829, doi: 10.1016/j.colsurfa.2021.126829.
[25] J.J. Wang, J. Wei, Functionalization of loofah fibers via surface-initiated AGET ATRP for synergic adsorption of multiple pollutants from water, Mater. Lett., 210 (2018) 214–217.
[26] K. Khezri, Y. Fazli, Evaluation of the effect of hydrophobically modified silica aerogel on the ARGET ATRP of styrene and butyl acrylate, Microporous Mesoporous Mater., 280 (2019) 236–242.
[27] A. Gopinath, A. Sultan Nasar, Fluorescent star ATRP initiators and fluorescent star poly(methyl methacrylate)s: synthesis and photophysical properties, Polymer, 153 (2018) 139–149.
[28] M.K. Uddin, R.A.K. Rao, K.V.V. Chandra Mouli, The artificial neural network and Box–Behnken design for Cu2+ removal by the pottery sludge from water samples: equilibrium, kinetic and thermodynamic studies, J. Mol. Liq., 266 (2018) 617–627.
[29] A. Khatoon, M.K. Uddin, R.A.K. Rao, Adsorptive remediation of Pb(II) from aqueous media using *Schleichera oleosa* bark, Environ. Technol. Innovation, 11 (2018) 1–14.
[30] M. Hassan, R. Naidu, J.H. Du, F.J. Qi, A. Ahsan, Y.J. Liu, Magnetic responsive mesoporous alginate/β-cyclodextrin polymer beads enhance selectivity and adsorption of heavy metal ions, Int. J. Biol. Macromol., 207 (2022) 826–840.
[31] H. Azad, M. Mohsennia, C. Cheng, A. Amini, Facile fabrication of PVB-PVA blend polymer nanocomposite for simultaneous removal of heavy metal ions from aqueous solutions: kinetic, equilibrium, reusability and adsorption mechanism, J. Environ. Chem. Eng., 9 (2021) 106214, doi: 10.1016/j.jece.2021.106214.
[32] Jumina, Y. Priastomo, H.R. Setiawan, Mutmainah, Y.S. Kurniawan, K. Ohto, Simultaneous removal of lead(II), chromium(III), and copper(II) heavy metal ions through an adsorption process using C-phenylcalix[4]pyrogallolarene material, J. Environ. Chem. Eng., 8 (2020) 103971, doi: 10.1016/j.jece.2020.103971.
[33] R.A.K. Rao, M. Kashifuddin, Adsorption studies of Cd(II) on ball clay: comparison with other natural clays, Arabian J. Chem., 9 (2016) S1233–S1241, doi: 10.1016/j.arabjc.2012.01.010.
[34] R.A.K. Rao, S. Ikram, M.K. Uddin, Removal of Cr(VI) from aqueous solution on seeds of *Artimisia absinthium* (novel plant material), Desal. Water Treat., 54 (2015) 3358–3371.
[35] H.P. Wang, T. Wang, R.R. Ma, K. Wu, H.L. Li, B. Feng, C. Li, Y.H. Shen, Facile synthesis of sulfonated covalent organic framework for the adsorption of heavy metal ions, J. Taiwan Inst. Chem. Eng., 112 (2020) 122–129.
[36] H.B. Jiang, Y.R. Yang, Z.K. Lin, B.C. Zhao, J. Wang, J. Xie, A.P. Zhang, Preparation of a novel bio-adsorbent of sodium alginate grafted polyacrylamide/graphene oxide hydrogel for the adsorption of heavy metal ion, Sci. Total Environ., 744 (2020) 140653, doi: 10.1016/j.scitotenv.2020.140653.